

# Is the IMF in ellipticals bottom-heavy? Clues from their chemical abundances.

C. De Masi,<sup>1\*</sup> F. Vincenzo,<sup>2</sup> F. Matteucci,<sup>1,3,4</sup> G. Rosani,<sup>5,6</sup> F. La Barbera,<sup>7</sup>  
A. Pasquali<sup>5</sup> E. Spitoni<sup>1</sup>

<sup>1</sup> *Astronomy Department, University of Trieste, Via Tiepolo 11, I-34127 Trieste, Italy*

<sup>2</sup> *Centre for Astrophysics Research, School of Physics, Astronomy and Mathematics, University of Hertfordshire, College Lane, Hatfield, AL10 9AB, UK*

<sup>3</sup> *I.N.A.F. Osservatorio Astronomico di Trieste, via G.B. Tiepolo 11, I-34131, Trieste, Italy*

<sup>4</sup> *I.N.F.N. Sezione di Trieste, via Valerio 2, 34134 Trieste, Italy*

<sup>5</sup> *Astronomisches Rechen-Institut, Zentrum für Astronomie, Universität Heidelberg, Mönchhofstr. 12-14, D-69120 Heidelberg, Germany*

<sup>6</sup> *Kapteyn Astronomical Institute, University of Groningen, P.O. Box 800, 9700AV Groningen, The Netherlands*

<sup>7</sup> *INAF - Astronomical Observatory of Capodimonte, via Moiariello 16, 80131 Napoli, Italy*

Accepted XXX. Received YYY; in original form ZZZ

## ABSTRACT

We tested the implementation of different IMFs in our model for the chemical evolution of ellipticals, with the aim of reproducing the observed relations of  $[\text{Fe}/\text{H}]$  and  $[\text{Mg}/\text{Fe}]$  abundances with galaxy mass in a sample of early-type galaxies selected from the SPIDER-SDSS catalog. Abundances in the catalog were derived from averaged spectra, obtained by stacking individual spectra according to central velocity dispersion, as a proxy of galaxy mass. We tested initial mass functions already used in a previous work, as well as two new models, based on low-mass tapered (“bimodal”) IMFs, where the IMF becomes either (1) bottom-heavy in more massive galaxies, or (2) is time-dependent, switching from top-heavy to bottom-heavy in the course of galactic evolution. We found that the best agreement between models and observations is given either by models with a constant, Salpeter IMF, or by those with a time-dependent distribution. We further tested the models by calculating their M/L ratios. We conclude that a constant, time-independent bottom-heavy IMF does not reproduce the data, especially the increase of the  $[\alpha/\text{Fe}]$  ratio with galactic stellar mass, whereas a variable IMF, switching to bottom-heavy at late times can match observations.

**Key words:** galaxies: abundances – galaxies: elliptical and lenticular, cD – galaxies: evolution – galaxies: formation – galaxies: luminosity function, mass function

## 1 INTRODUCTION

The initial mass function (IMF) deeply affects the chemical evolution of a galaxy on many different levels, by determining the ratio between low and high mass stars.

The former are known to produce the bulk of Fe in the galaxy via type Ia SNe over long time scales (Matteucci & Greggio 1986; Matteucci & Recchi 2001); additionally, even when not directly influencing the chemical abundances over a Hubble time, they still affect their evolution by locking away baryonic matter from the interstellar medium. On the opposite end of the mass range, massive stars are the main producers of  $\alpha$  elements (O, Mg, Si, Ca), via processes characterized

by much shorter timescales than for Fe-peak elements. The difference in production channels and timescales of the various chemical elements from stars in different mass ranges, when combined with the star formation history of a galaxy, leaves a characteristic mark on abundance ratios such as the  $[\alpha/\text{Fe}]$ , which in turn may allow the formation history itself to be reconstructed from observations (Matteucci 1994; Matteucci et al. 1998; Matteucci 2012).

Other than the chemical evolution, many other properties of a galaxy are strictly related to the IMF. Low mass stars mainly contribute to build up the total present time stellar mass (Kennicutt 1998), while massive stars dominate the integrated light of galaxies (Conroy & van Dokkum 2012b), and determine the amount of energetic feedback produced after star formation episodes. Generally, different proper-

\* E-mail: demasi@oats.inaf.it

ties are determined by the slope of the IMF in different mass ranges. [Renzini & Greggio \(2012\)](#) investigated the topic thoroughly, and showed how the slope below  $\approx 1 M_{\odot}$  dominates the M/L ratio in local ellipticals, while its evolution is mainly influenced by the slope between  $\approx 1$  and  $\approx 1.4 M_{\odot}$ . For these reasons, it does not come as a surprise that determining the exact shape of the IMF is one of the focal points of interest in the study of galaxies. Theoretically, a comprehensive physical picture explaining the origin and properties of the IMF does not exist yet; to this regard, [Silk \(1995\)](#); [Krumholz \(2011\)](#) analyzed the effect of molecular flows and protostellar winds, [Larson \(1998, 2005\)](#) tried to explain it in terms of the Jeans mass, while [Bonnell et al. \(2007\)](#); [Hopkins \(2013\)](#); [Chabrier et al. \(2014\)](#) explored the effect of gravitational fragmentation and of the thermal physics.

Observationally, direct star counts in star forming regions and clusters of our Galaxy all seemed to point towards an invariant IMF, characterized as a Kroupa/Chabrier distribution, with a power-law for  $m > 1M_{\odot}$ , and a turn-off at lower masses ([Scalo 1986](#); [Kroupa 2001, 2002](#); [Bastian et al. 2010](#); [Kroupa et al. 2013](#)); this, in turn, generally led to the assumption of the universality of the IMF. A direct verification of this assumption, however, is well beyond our current observational capabilities, so that we are bound to employ indirect methods to obtain constraints on the IMF of galaxies with unresolved stellar populations. The main approach is that of observing gravity-sensitive features in the galaxy integrated spectra; to name a few, the presence of the NaI $\lambda$ 8183, 8195 doublet lines and of the Wing-Ford FeH band at 9900 Å is an indicator of the presence of low-mass dwarfs, while the Ca triplet lines at  $\lambda$ 8498, 8542, and 8662 Å are strong in giants and basically undetectable in dwarfs ([Wing & Ford 1969](#); [Faber & French 1980](#); [Diaz et al. 1989](#)). A number of works involving the observation of these features provided indications for the IMF becoming bottom-heavier than a Kroupa/Chabrier in massive early-type galaxies. [Cenarro et al. \(2003\)](#) first proposed a trend towards an excess of low-mass stars in massive galaxies, from a study of the CaT region. [van Dokkum & Conroy \(2010, 2011\)](#) came to the same conclusion after analyzing a sample of eight massive ETGs in the Virgo and Coma clusters, and further confirmed it by using stellar population models accounting for variable element abundance ratios and using a full spectral fitting analysis on a set of 34 ETGs from the SAURON survey ([Conroy & van Dokkum 2012a,b](#)). [Ferrerias et al. \(2013\)](#); [La Barbera et al. \(2013\)](#), as well as [Spiniello et al. \(2014\)](#) showed that a systematic trend is in place for the whole population of ETGs, with higher velocity dispersion (mass) galaxies having a bottom-heavier IMF (but see also [Smith & Lucey 2013](#); [Smith et al. 2015](#); [Newman et al. 2017](#) for evidence of some massive ETGs with a "light" IMF normalization). A similar result was claimed by [Auger et al. \(2010\)](#); [Grillo & Gobat \(2010\)](#); [Treu et al. \(2010\)](#); [Barnabè et al. \(2011\)](#); [Cappellari et al. \(2012\)](#); [Spiniello et al. \(2012\)](#) on the basis of kinematics and gravitational lensing studies, and by [Dutton et al. \(2011, 2012, 2013\)](#) from scaling relations and models of light and dark-matter distribution in galaxies.

On the other hand, however, [Gunawardhana et al. \(2011\)](#) observed a strong dependence of the IMF on star formation in a sample of low-to-moderate star-forming galaxies redshift galaxies from the GAMA survey, with the high mass slope of

the initial mass function becoming flatter (hence providing a top-heavier IMF) in objects with higher formation activity, as it might be the case for the progenitors of more massive galaxies ([Matteucci et al. 1998](#); [Matteucci 2012](#)).

Historically, galaxy formation models based on the hierarchical scenario failed in simultaneously reproducing two fundamental observational features of ellipticals, i.e. the increase of the  $[\alpha/Fe]$  ratios with higher values of  $\sigma$  (a proxy for mass) and the mass-metallicity relation ([Pipino & Matteucci 2008](#); [Okamoto et al. 2017](#)). Common solutions proposed to overcome this limit generally involved the introduction of AGN feedback and/or of variable IMFs, becoming top-heavier with mass.

In this sense, [Thomas et al. \(1999\)](#) proposed two scenarios for the formation of giant ellipticals, either via fast ( $\approx 1Gyr$ ) collapse of smaller entities or via merging of spiral galaxies similar to the Milky Way; in the latter case, the desired  $[\alpha/Fe]$  overabundance could only be reproduced by assuming an IMF flatter than a Salpeter during the initial starburst triggered by the merging.

Similarly, a combination of IMFs top-heavier than a Salpeter one with other mechanisms was proposed by [Calura & Menci \(2009\)](#), who assumed a star-formation-dependent IMF - with a slope switching from a Salpeter ( $x=1.35$ ) to a slightly flatter value ( $x=1$ ) for  $SFR > 100M_{\odot} yr^{-1}$  - together with interaction-triggered starbursts and AGN feedback. [Arrigoni et al. \(2010\)](#) used both a top-heavy IMF (with a slope  $x = 1.15$ ) and a lower SNe Ia ratio. [Gargiulo et al. \(2015\)](#) implemented SFR-dependent IMF together with a radio-mode AGN feedback quenching star formation. To conciliate the opposing indications as to whether the IMF in more massive ellipticals should be bottom or top-heavy, [Weidner et al. \(2013\)](#); [Ferrerias et al. \(2015\)](#) proposed a time dependent form of the IMF, switching from a top-heavier form during the initial burst of star formation to a bottom-heavier one at later times.

In [De Masi et al. \(2018\)](#), we studied the chemical patterns observed in a sample of elliptical galaxies by adopting the chemical evolution model presented in [Pipino & Matteucci \(2004\)](#), describing the detailed time evolution of 21 different chemical elements. In that work, we generated the model galaxies by fine-tuning their initial parameters (star formation efficiency, infall time scale, effective radius and IMF) for different values of the mass, which yielded constraints on the formation and evolution of elliptical galaxies. Specifically, in accordance to the "inverse wind scenario" ([Matteucci 1994](#)), we found that the best fitting models were those with higher star formation efficiency, larger effective radius and lower infall time scale in more massive galaxies. Moreover, at variance with what was concluded in [Matteucci \(1994\)](#), we observed the necessity for a variation in the IMF as well, becoming top-heavier in more massive galaxies.

In this paper, we adopt a new dataset for the comparison, and we follow a different approach in generating the models, with the aim of better exploring the available parameter space. Instead of manually fine-tuning the parameters of the models, we assumed a parameterization for the IMF, and for each choice of the latter we generated the models by varying all the initial parameters over a grid of values (see tables 1 and 2).

This paper is organized as follows.

In section 2, we present the adopted dataset, in section 3

**Table 1.** Possible values of the initial parameters used to generate the model galaxies in the time-independent cases (Models 01-04). For each choice of the IMF, we generated model galaxies using all the possible combinations of values reported in this table.

Parameter	Value
Infall mass ( $M_{\odot}$ )	$5 \times 10^9, 9 \times 10^9, 1.62 \times 10^{10}, 2.92 \times 10^{10}, 5.25 \times 10^{10}, 9.45 \times 10^{10}, 1.70 \times 10^{11}, 3.06 \times 10^{11}, 5.51 \times 10^{11}, 9.92 \times 10^{11}, 1.79 \times 10^{12}$
Effective radius (kpc)	1, 2, 3, 4, 5, 6, 7, 8, 9, 10
Star formation efficiency $\nu$ ( $Gyr^{-1}$ )	5, 10, 15, 20, 25, 30, 35, 40, 45, 50
Infall time-scale $\tau$ ( $Gyr$ )	0.2, 0.3, 0.4, 0.5

**Table 2.** Possible values of the initial parameters used to generate the model galaxies in the time-dependent case (Model 05; see text). We generated model galaxies using all the possible combinations of values reported in this table.

Parameter	Value
Infall mass ( $M_{\odot}$ )	$5 \times 10^9, 9 \times 10^9, 1.62 \times 10^{10}, 2.92 \times 10^{10}, 5.25 \times 10^{10}, 9.45 \times 10^{10}, 1.70 \times 10^{11}, 3.06 \times 10^{11}, 5.51 \times 10^{11}, 9.92 \times 10^{11}, 1.79 \times 10^{12}$
Effective radius (kpc)	1, 3, 5, 7, 9, 11
Star formation efficiency $\nu$ ( $Gyr^{-1}$ )	5, 10, 20, 30, 40, 50
Infall time-scale $\tau$ ( $Gyr$ )	0.2, 0.5
$\mu_1$	0.4, 0.7, 1.0, 1.3
$\mu_2$	1.3, 1.6, 1.9, 2.3, 2.6, 2.9
$t_{switch}$ ( $Gyr$ )	0.1, 0.3, 0.5, 0.8, 1.0

we describe our chemical evolution model, focusing on the comparison with the observed quantities, and describe the properties of the various adopted forms of the IMF.

In section 4, we summarize the results of this work, indicating the IMFs which can provide the best fit to the dataset. Finally, in section 5 we present the analysis we performed on the calculation of the M/L ratios predicted by our best-fitting models, in an attempt to obtain further constraints.

## 2 DATASET

The dataset used in this work is a subsample of the catalogue of ETGs presented in La Barbera et al. (2010).

Details on the selection of the general dataset can be found in La Barbera et al. (2013) and the final state of the dataset used in this work can be found in (Rosani et al. 2018, hereafter R18). Briefly, we analyze stellar galaxy properties inferred from spectra stacked in central velocity dispersion from 20996 ( $0.05 < z < 0.095$ ) early-type galaxies, extracted from the 12th Data Release of the SDSS. The stacked spectra were collected to ensure a S/N ratio of the order of a few hundreds, needed to obtain constraints on the IMF from gravity-sensitive features Conroy & van Dokkum (2012a). The environment information for the galaxies in the dataset are derived from the catalog of Wang et al. (2014).

As detailed in R18, stellar population properties and chemical abundances for various elements have been derived from the stacked spectra by fitting the equivalent widths of a set of line indices to the equivalent widths predicted by synthetic stellar population (SSP) models. The models used for the fitting are the EMILES SSPs of Vazdekis et al. (2016), with variable IMF slope, age, and total metallicity. Two approaches have been explored in the fitting by R18: i) the case in which only age, metallicity and IMF-sensitive indices were used; ii) the case in which, additionally to the ones of the previous case, indices sensitive to abundance pattern of different elements (among which  $[Mg/Fe]$ ) were used. In this work, the values of IMF slope, age and total metallicity

$[Z/H]$  used are those derived by R18 for case i).

Since ETGs are found to be not solar-scaled in abundance pattern, but the EMILES models are, the abundances obtained in the fit for each stacked spectrum had to be corrected to reflect the  $\alpha$ -enhancement of ETGs. To this purpose, R18 calculated an  $[Mg/Fe]$  proxy (as detailed in La Barbera et al. (2013)) using the difference between the metallicity derived from the  $Mgb5177$  index and the metallicity derived using the  $Fe3$  index (see Trager et al. (1998) and Kuntschner (2000) respectively for index definition). Since this value of  $[Mg/Fe]$  is not linked to the way the SSP models are computed, but only to the data, we regard this as more secure and use it for our comparison.

Finally, to obtain  $[Fe/H]$  for each of the stacked spectra, we inverted the relation linking  $[Mg/Fe]$ ,  $[Fe/H]$  and total metallicity (see Vazdekis et al. (2015) for details, as well as for a discussion on the factor 0.75 used in the equation below):

$$[Z/H] = [Fe/H] + 0.75 \times [Mg/Fe]. \quad (1)$$

Both the  $[Fe/H]$  and the  $[Mg/Fe]$  abundances have been compared to the analogous ratios as directly predicted by our chemical evolution code. Specifically, we used these values to test the mass-metallicity and  $[Mg/Fe]$ -mass relation predicted by our chemical evolution model.

In Figure 1, we show the variation of  $[Fe/H]$  and  $[Mg/Fe]$  as a function of galaxy mass in the SDSS stacked spectra, with their  $1-\sigma$  uncertainties. Since the stacking in R18 is originally performed in central velocity dispersion ( $\sigma_0$ ) bins, we derived the stellar mass associated to a given stacked spectrum. Specifically, we took the stellar masses listed in the group catalog of Wang et al. (2014); as described by Yang et al. (2007), stellar masses are derived from the relation between stellar mass- to-light ratio and colour of Bell et al. (2003).

Both  $[Fe/H]$  and  $[Mg/Fe]$  exhibit a clear positive correlation with mass, in agreement with theoretical expectations, and consistently to what observed in literature (Trager et al. 2000; Thomas et al. 2005; Bernardi et al. 2006; Graves &

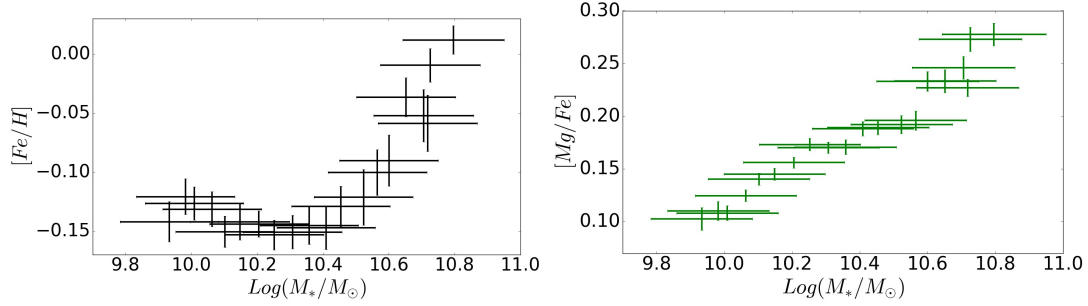


**Figure 1.**  $[Fe/H]$  and  $[Mg/Fe]$  ratios variation with stellar mass in the 20 mass bins provided in the dataset.

Schiavon 2008; Thomas et al. 2010; Johansson et al. 2012; Conroy et al. 2014).

### 3 MODELS

In this section, we present the implementation of our chemical evolution model. We start by giving a brief description of the model itself, of the calibrations needed to compare the results with the data, and we present the various forms of the IMF we tested in this work.

#### 3.1 Chemical evolution model

A detailed description of the chemical evolution model adopted in this paper can be found in Pipino & Matteucci (2004) and De Masi et al. (2018). Here, we briefly summarize its properties.

The model follows the detailed evolution with time of 21 different chemical elements in the various shells the galaxy is divided, by solving the equation of chemical evolution (CEQ - Matteucci & Greggio 1986; Matteucci & Gibson 1995) for each of the elements:

$$\begin{aligned}
 \frac{dG_i(t)}{dt} = & -\psi(t) X_i(t) + \\
 & + \int_{0.8M_\odot}^{3M_\odot} \psi(t - \tau_m) Q_{mi}(t - \tau_m) \varphi(m) dm + \\
 & + A \int_{3M_\odot}^{16M_\odot} dm \varphi(m) \times \\
 & \times \left[ \int_{\mu_m}^{0.5} f(\mu) \psi(t - \tau_{m_2}) Q_{mi}(t - \tau_{m_2}) d\mu \right] + \\
 & + (1 - A) \int_{3M_\odot}^{16M_\odot} \psi(t - \tau_m) Q_{mi}(t - \tau_m) \varphi(m) dm + \\
 & + \int_{16M_\odot}^{M_U} \psi(t - \tau_m) Q_{mi}(t - \tau_m) \varphi(m) dm + \\
 & + \left[ \frac{dG_i(t)}{dt} \right]_{infall}
 \end{aligned} \tag{2}$$

where each of the four integrals provides the quantity of the  $i$ -th chemical element restored to the ISM by dying stars of various masses. Single stars (both in the  $0.8 M_\odot - 3 M_\odot$  and the  $3 M_\odot - 16 M_\odot$  mass ranges), binary systems generating type Ia SNe (with total mass  $M_{B_m}$  in the  $3 M_\odot - 16 M_\odot$

range), and core collapse SNe ( $m > 16 M_\odot$ ).

In the second integral, we made use of the Type Ia SNe rate for the single degenerate scenario (Whelan & Iben 1973) as defined in Greggio & Renzini (1983); Matteucci & Greggio (1986); Matteucci & Recchi (2001):

$$R_{SNIa} = A \int_{M_{B_m}}^{M_{B_M}} dM_B \varphi(M_B) \int_{\mu_m}^{0.5} f(\mu) \psi(t - \tau_m) d\mu \tag{3}$$

The mass fraction of the secondary star (the originally least massive one) with respect to the total mass of the binary system  $\mu \equiv M_2/M_B$  is distributed according to:

$$f(\mu) = 2^{\gamma+1} (\gamma + 1) \mu^\gamma \tag{4}$$

with  $\gamma = 2$ , and the free parameter  $A$  is constrained in order to reproduce the present-day observed rate of Type Ia SNe (Cappellaro et al. 1999).

The core-collapse SNe rate is

$$\begin{aligned}
 R_{cc} = & (1 - A) \int_8^{16} dm \varphi(m) \psi(t - \tau_m) + \\
 & + \int_{16}^{M_{WR}} dm \varphi(m) \psi(t - \tau_m) + \\
 & + \int_{M_{WR}}^{M_U} dm \varphi(m) \psi(t - \tau_m) + \\
 & + \alpha_{Ib/c} \int_{12}^{20} \varphi(m) \psi(t - \tau_m)
 \end{aligned} \tag{5}$$

where the first two integrals provide the Type II SNe rate, while the third and the fourth one express the Type Ib/c SN rate for single stars and binary systems, respectively. Again,  $\alpha_{Ib/c}$  is a free parameter, representing the fraction of stars in the considered mass range which can actually produce Type Ib/c SNe, and its value is modified to reproduce the observed rate.

The quantity:

$$X_i(t) \equiv \frac{M_i}{M_{gas}}$$

is the abundance by mass of the  $i$ -th chemical species in the ISM, with the normalization

$$\sum_{i=1}^N X_i = 1$$

while

$$G_i(t) = X_i(t) \rho_{gas}(t) \tag{6}$$

is the ratio between the mass density of the element  $i$  at the time  $t$  and its initial value.

The star formation rate  $\psi(t)$  is assumed to be described by a Kennicutt law (Kennicutt 1998), until the time at which the thermal energy, injected from stellar winds and SNe, overcomes the binding energy of the gas. At this point, a galactic wind starts, driving away the residual gas and quenching the star formation (Larson 1974; Pipino & Matteucci 2004):

$$\psi(t) = \begin{cases} \nu \rho_{gas}(t) & \text{before GW} \\ 0 & \text{after GW} \end{cases} \quad (7)$$

with a star formation efficiency  $\nu$  getting higher in more massive galaxies (“inverse wind model” - Matteucci 1994; Matteucci et al. 1998). In order to determine the thermal energy in the ISM and the time of the onset of the galactic wind, the code evaluates the contribution of both Type I and II SNe, assuming an average efficiency of energy release of the  $\approx 20\%$  between the two types (Cioffi et al. 1988; Recchi et al. 2001; Pipino et al. 2002).

The assumed stellar yields are the same adopted in Pipino & Matteucci (2004); De Masi et al. (2018).

### 3.2 Comparison between data and model output

As detailed in De Masi et al. (2018), a comparison between the results of our chemical evolution model and data is in general only possible after taking an additional step. Specifically, chemical abundance estimates in ellipticals are mainly determined by the composition of stars dominating the visual light of the galaxy, whereas our code provides the evolution with time of the abundances in the ISM. From the latter quantity, one has to perform an average, either on mass or luminosity (the results are not significantly different in massive galaxies; see Matteucci et al. 1998), to obtain an estimate of the chemical composition of the dominant stellar population. Specifically, in this work we applied the prescription by Pagel & Patchett (1975), where the mass average is defined as:

$$\langle X/H \rangle_{mass} \equiv \frac{1}{M_0} \int_0^{M_0} Z(M) dM \quad (8)$$

where  $M_0$  is the total mass of stars ever born contributing to light at the present time. Using equation 8 allows us to obtain abundance predictions that can be compared to the observed ones.

### 3.3 Adopted IMFs

In this paper, we expand the investigation of the effects of different IMFs on the evolution of elliptical galaxies we previously carried out in De Masi et al. (2018), by testing the IMF parameterizations adopted in the previous paper, as well as some new IMF models.

Specifically, the adopted IMFs are:

- **Model 01:**

We obtained these galaxy models by using a fixed (Salpeter 1955) IMF and by considering all possible combinations of values reported in Table 1 for the initial parameters.

In figure 2, we show the variation of the  $[Fe/H]$  and  $[Mg/Fe]$  abundance ratios with stellar mass, as calculated by the chemical evolution code for all model galaxies; for each ratio, we provide three versions of the same plot, color

coded to show the effect of varying the star formation efficiency  $\nu$ , the infall time scale  $\tau$  and the effective radius  $R_{eff}$ , respectively. It is evident how the  $[Mg/Fe]$  ratio in galaxies of the same stellar mass are higher in models with increasing  $\nu$ , where the larger thermal energy injected by stellar winds and SNe into the ISM leads to an earlier onset of a galactic wind, which drives the gas away from the galaxy and quenches star formation.

The effect of decreasing the infall time scale  $\tau$ , which is similar to increasing  $\nu$  and  $R_{eff}$ , appears to be less significant.

- **Model 02:**

In De Masi et al. (2018), we applied the prescriptions of the “inverse wind” model (Matteucci 1994; Matteucci et al. 1998; Matteucci 2012), where the star formation process is more efficient and shorter in more massive galaxies, to reproduce the higher  $[\alpha/Fe]$  observed in more massive galaxies (“downsizing” in star formation). This assumption, however, proved to be insufficient to reproduce the slope of the observed trends (De Masi et al. 2018), so that we decided to test a variable IMF, switching to different parameterizations in different mass ranges; specifically, the IMF variation which provided the best results was:

- **Scalo (1986):** we used the approximate expression adopted in Chiappini et al. (1997):

$$\varphi(m) \propto \begin{cases} m^{-2.35} & 0.1 \leq m/M_\odot < 6 \\ m^{-2.7} & 6 \leq m/M_\odot \leq 100 \end{cases} \quad (9)$$

- **Salpeter (1955)**, which is a simple power-law:

$$\varphi(m) \propto m^{-2.35} \quad 0.1 \leq m/M_\odot < 100 \quad (10)$$

- **Chabrier (2003):**

$$\varphi(m) \propto \begin{cases} e^{-\frac{(\text{Log}(m) - \text{Log}(0.079))^2}{2(0.69)^2}} & 0.1 \leq m/M_\odot < 1 \\ m^{-2.2} & 1 \leq m/M_\odot \leq 100 \end{cases} \quad (11)$$

Models 02 are produced by assuming the same IMF variation, as well as the parameters value reported in Table 1. As for the previous Model, in figure 3 we show the values of  $[Fe/H]$  and  $[Mg/Fe]$  abundance ratios, as a function of stellar mass and with a color coding indicating the dependence on star formation efficiency, infall time-scale and effective radius.

- **Model 03:**

In these Models, we tested the effect of assuming an Integrated Galactic IMF (Recchi et al. 2009; Vincenzo et al. 2014; Weidner et al. 2010).

The IGIMF is obtained by combining the IMF describing the mass distribution of new-born stars within the star clusters - where star formation is assumed to take place - with the mass distribution of star clusters themselves (embedded cluster mass function, ECMF); assuming for the latter the form (with  $\beta \approx 2$ )

$$\xi_{ecl} \propto M_{ecl}^\beta \quad (12)$$

the IGIMF is then defined as (Weidner et al. 2011; Vincenzo et al. 2015):

$$\begin{aligned} \xi_{IGIMF}(m, t) &\equiv \\ &\equiv \int_{M_{ecl}^{min}}^{M_{ecl}^{max}(\psi(t))} \varphi(m < m_{max}(M_{ecl})) \xi_{ecl}(M_{ecl}) dM_{ecl} \end{aligned} \quad (13)$$

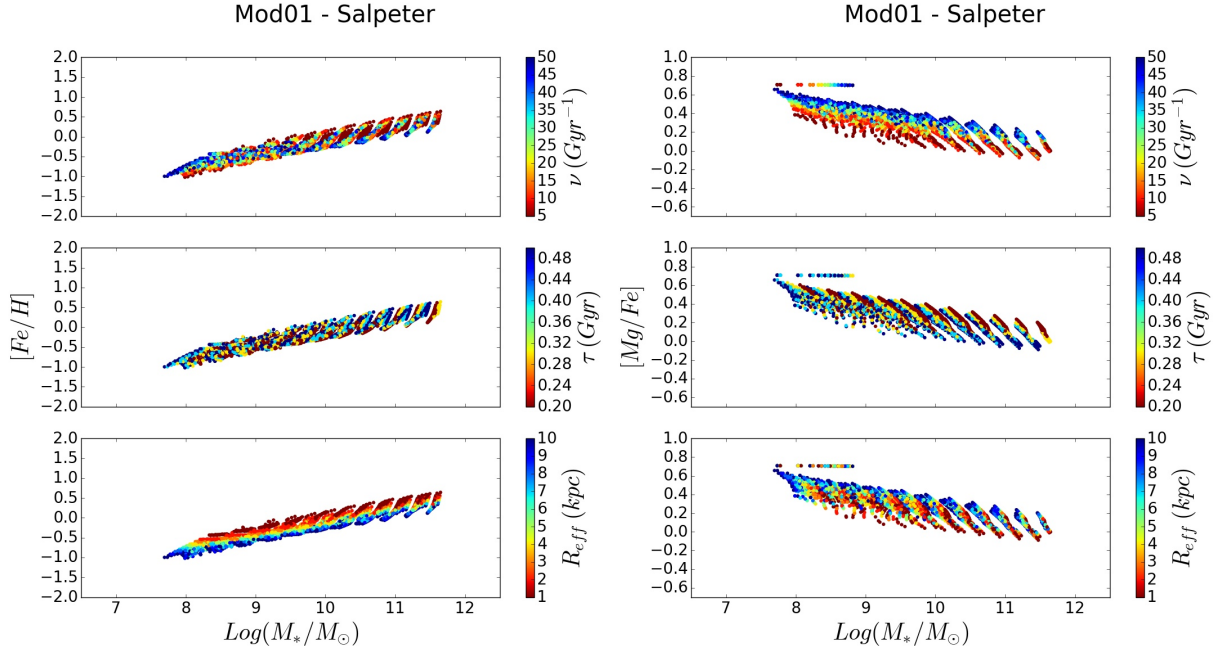


**Figure 2.**  $[Fe/H]$  and  $[Mg/Fe]$  ratios (left and right panel, respectively) for 4400 model galaxies, obtained by varying the model initial parameters over the grid of values reported in table 1, and assuming a fixed Salpeter IMF (Models 01). The plots show the variation of chemical abundances with total stellar mass, and are color coded to further show the dependence on the star formation efficiency  $\nu$  (top panels), infall time-scale  $\tau$  (central panels) and effective radius  $R_{eff}$  (bottom panels).

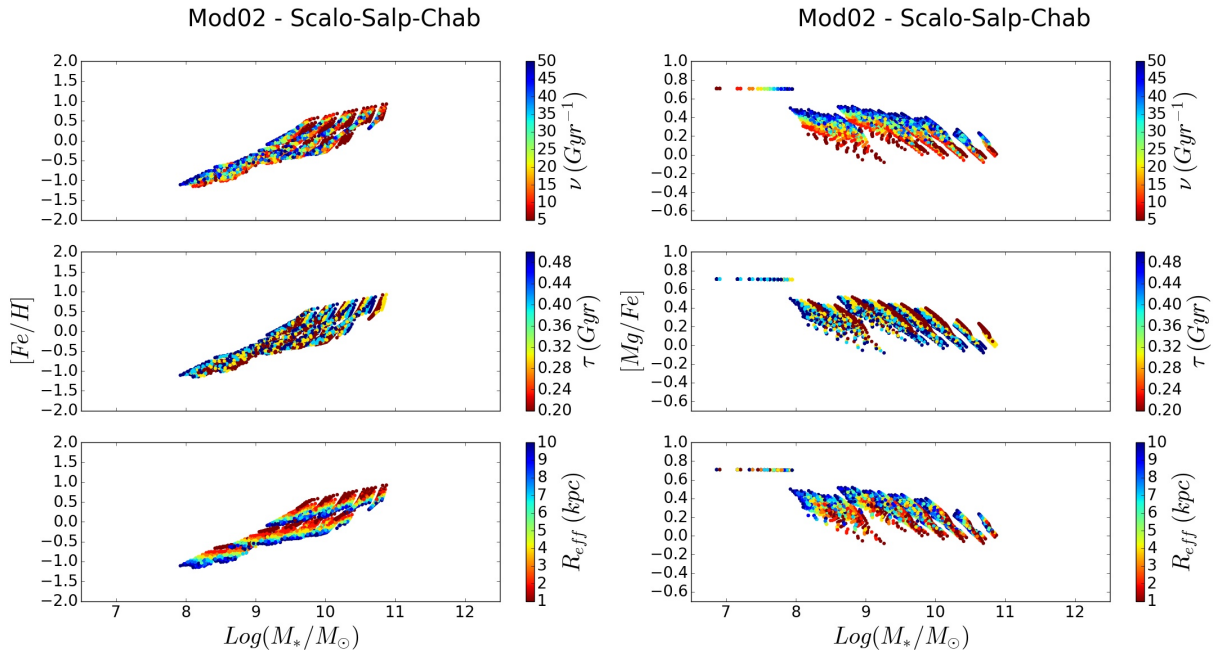


**Figure 3.** Same as figure 2, but for Model 02, where we assume an IMF that varies with galaxy mass, becoming top-heavier in more massive galaxies (see sec. 3.3).

with the mass normalization:

$$\int_{m_{min}}^{m_{max}} dm m \xi_{IGIMF}(m) = 1 \quad (14)$$

Briefly, for higher SFR values  $M_{ecl}^{max}$ , the maximum mass of the stellar clusters where star formation is taking place, increases, and hence the maximum mass of stars that can

be formed within the cluster is larger as well; defined this way, the IGIMF becomes top-heavier as the SFR increases. This is shown in figure 4, where we compare the IGIMF for different star formation rates (SFRs), with the Salpeter IMF.

Figure 5 shows the properties of these Models.

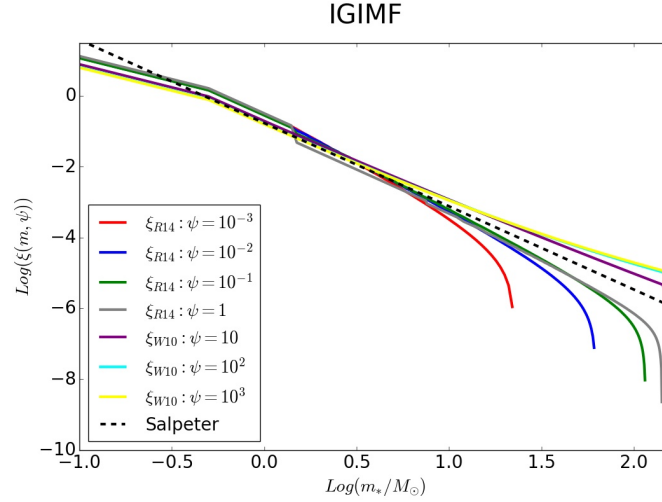


**Figure 4.** IGIMF for different SFRs (solid colours lines) and a canonical Salpeter IMF (black dashed line).

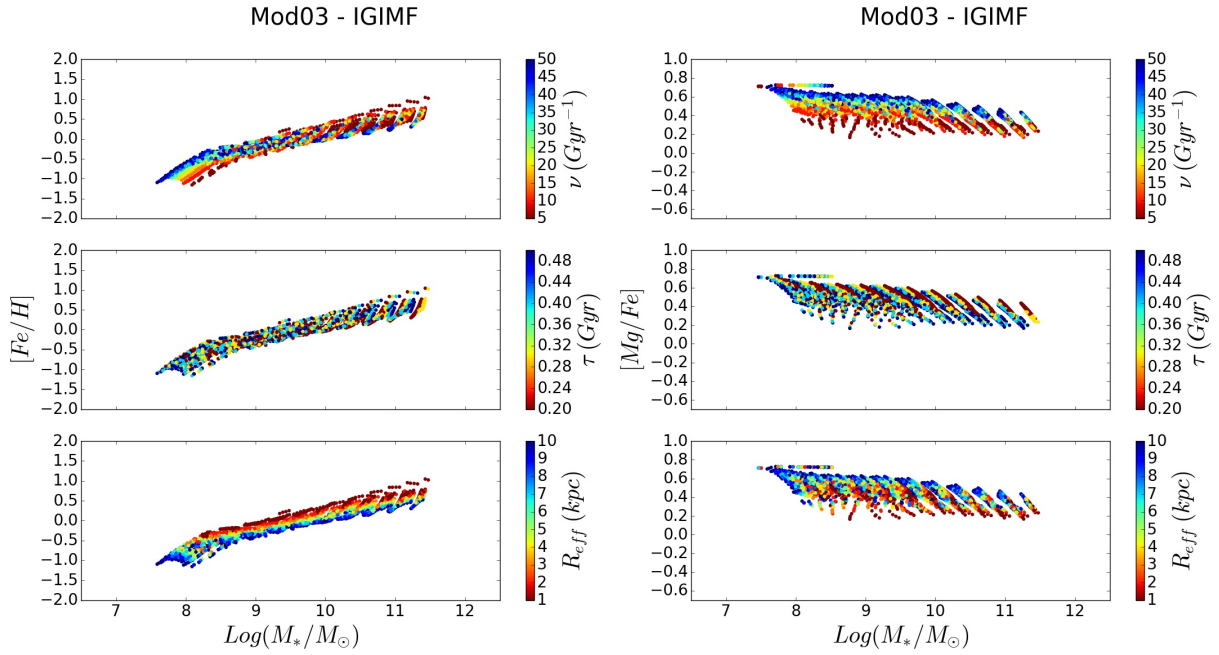


**Figure 5.** Same as figures 2 and 3, for Models 03 assuming an IGIMF, becoming top-heavier for higher SFR values in more massive galaxies (see sec. 3.3).

• **Model 04:**

In these models, we tested the effect of adopting a low-mass tapered (“bimodal”) IMF, as defined in Vazdekis et al. (1997, 2003).

In this formulation, the IMF is defined as

$$\xi(m) = \beta \begin{cases} m_1^{-\mu} & 0.1 < m/M_\odot < 0.2 \\ p(m) & 0.2 < m/M_\odot < 0.6 \\ m^{-\mu} & 0.6 < m/M_\odot < 100 \end{cases} \quad (15)$$

where  $m_1 = 0.4$ , and  $p(m)$  is a third degree spline, i.e.

$$p(m) = (A + Bm + Cm^2 + Dm^3) \quad (16)$$

whose normalization constants are determined by solving

the following boundary conditions:

$$\begin{cases} p(0.2) = m_1^{-\mu} \\ p'(0.2) = 0 \\ p(0.6) = 0.6^{-\mu} \\ p'(0.6) = -\mu 0.6^{(-\mu-1)} \end{cases}$$

Notice that for  $\mu = 1.3$ , the bimodal IMF closely matches a Kroupa distribution. For  $\mu > 1.3$ , this IMF becomes more and more bottom-heavy, while for  $\mu < 1.3$  the IMF is top-heavy. We tested the effects of the bimodal IMF by assuming an increasing value for the slope  $\mu$  (namely, a bottom heavier IMF) in more massive galaxies. Figure 6 compares the bimodal IMFs with those adopted in our previous work (i.e.

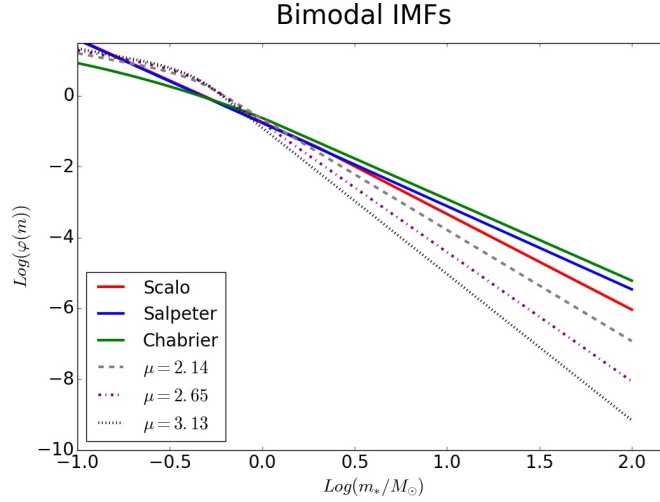


**Figure 6.** Comparison between bimodal IMF with varying slope  $\mu$ , and the IMFs used in our previous work (i.e. a Scalo, Salpeter, and Chabrier IMF; see the inset panel).

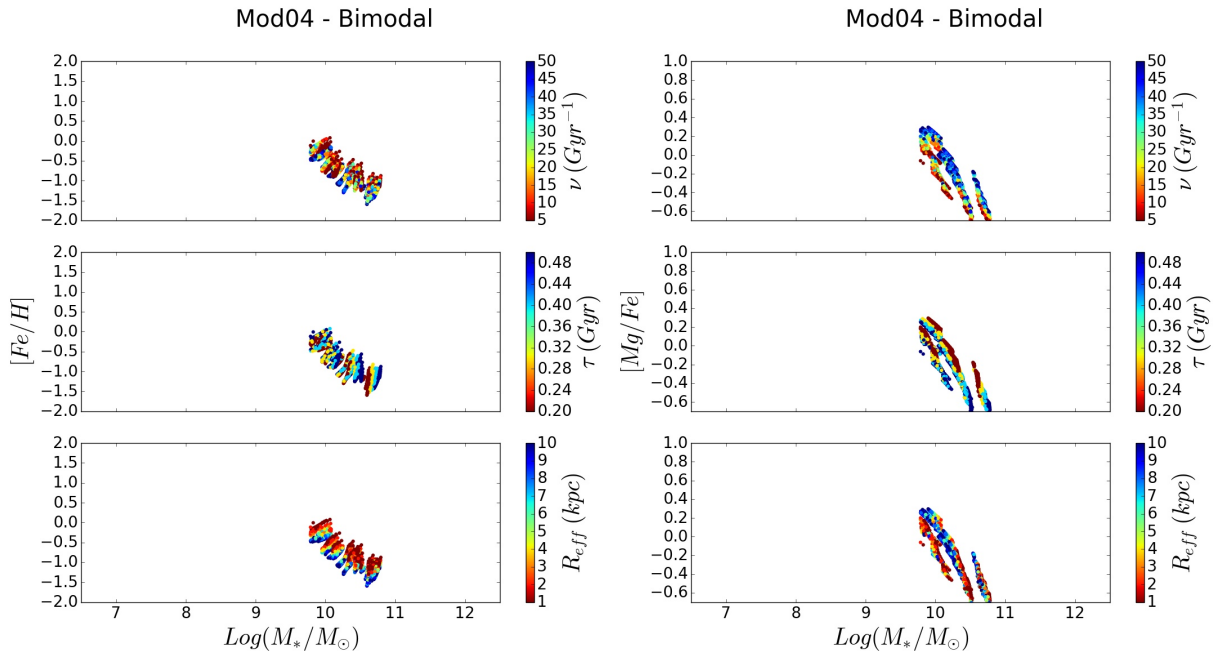


**Figure 7.** Same as figures 2, 3 and 5 for Model 04, obtained by assuming a bimodal IMF, becoming bottom-heavier in more massive galaxies (see sec. 3.3).

Models 01 and 02; see above). Figure 7 shows the dependence of the bimodal-IMF Models on  $\nu$ ,  $\tau$ ,  $R_{eff}$ .

- **Models 05:**

In this final set of models, we tested an explicitly time dependent form for the bimodal IMF, as described in Weidner et al. (2013); Ferreras et al. (2015), by assuming that the slope value  $\mu$  changes from an initial value  $\mu_1$  to a final value  $\mu_2$  after a time interval  $t_{switch}$  (the IMF switches from top to bottom-heavy, so that by construction  $mu_2 > mu_1$ ).

The Models are obtained by different combinations of  $\mu_1$ ,  $\mu_2$  and  $t_{switch}$  values, summarized in table 2.

In this way, we produced 95040 model galaxies, whose properties are illustrated in figure 8.

## 4 RESULTS

In this section, we compare predictions from different models with observations.

For every IMF, we selected Models matching the observed mass-[Fe/H] and mass-[Mg/Fe] relations within the observational errors.

The results of the matching procedure are summarized in figures 9 and 10 and in table 3. In all plots, galaxy models giving no matches are shown as gray points, while we highlight and color-code the acceptable models based on their star formation efficiency  $\nu$ .

For each IMF, table 3 reports the number of model galaxies matching the data, for three different mass ranges and in

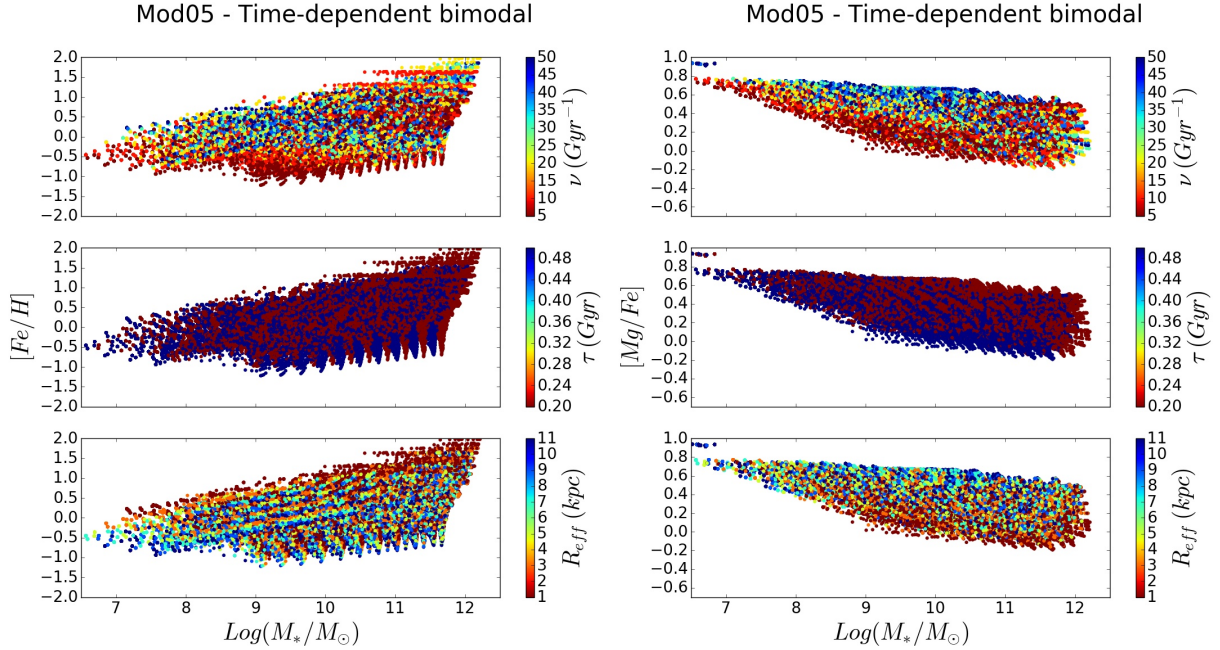


**Figure 8.** Same as figures 2, 3, 5 and 7, this time for models with an explicitly time-dependent bimodal IMF, becoming bottom-heavier in more massive galaxies (see sec. 3.3).

total, for the  $[Fe/H]$  ratio (columns 2-5), the  $[Mg/Fe]$  ratio (columns 6-9) and for both these quantities simultaneously (columns 10-13).

While all the suggested IMFs - aside from the IGIMF, which provided the worst results - produced model galaxies matching the abundance ratios of the data in the lower mass bin, the number of matches decreases dramatically at higher masses, especially for the  $[Fe/H]$  ratio. This happens for all the Models, except for the ones with a Salpeter (Models 01) or time-dependent bimodal IMFs (Models 05). Moreover, these two sets of Models were the only ones producing a significant number of matches for both the abundance ratios simultaneously.

For this reason, we selected from Models 01 and 05 the ones matching both  $[Fe/H]$  and  $[Mg/Fe]$ , and analyzed their properties.

In the case of the Salpeter IMF, we confirmed the results of Pipino & Matteucci (2004), with the best matching models presenting a trend of increasing star formation efficiency at higher masses (see fig. 11, left panel); on the other hand, this trend is mostly negligible with the time-varying bimodal IMF.

In Model 05, we observe that, despite the wide range of possible values for  $t_{switch}$  (the time at which the slope changes from the initial value  $\mu_1$  to the present day value  $\mu_2$ ), all model galaxies reproducing the two abundance ratios simultaneously switch slope at the same time; specifically, at  $t_{switch} = 0.1$  Gyr, the lowest value (for reference, Weidner et al. 2013 found the optimal time for the switch to be  $t_{switch} \geq 0.3$  Gyr). So, if the switch has to occur, it has to be in the early stages of the chemical evolution in order to reproduce the data.

A weak trend with mass can be observed in the slope value before and after the switch (see fig. 13 - top left panel). At low masses, we have mostly models with both  $\mu_1$  and

$\mu_2$  in the range from 1 to 2, i.e. not so different from the Kroupa-like slope (1.3). At highest masses, the slope before the switch  $\mu_1$  becomes as low as 0.5 (top-heavier), while the slope after the switch  $\mu_2$  gets as high as 2.6 (bottom-heavier). A plot of  $\mu_1$  vs  $\mu_2$  does not seem to show any significant correlation (fig. 13 - top right panel).

As described above, the only criteria applied in selecting the matching models was whether they matched the observed  $[Fe/H]$ -mass and the  $[Mg/Fe]$ -mass relations simultaneously, not taking into account other structural properties. However, a comparison between the effective radii of the models and the observed ones, as shown in figure 12, revealed that most of the models actually have an effective radius much bigger than the ones of the galaxies in the dataset, which allowed us to perform a further selection. So, limiting our analysis to models with effective radii matching the observed ones, we see that the trends discussed above of  $\mu_1$  and  $\mu_2$  with mass are still present (fig. 13 - bottom left panel); moreover, a weak correlation between  $\mu_1$  and  $\mu_2$  is present, pointing towards a scenario where a top-heavier IMF before the switch (lower  $\mu_1$  value) corresponds to a bottom-heavier one after the switch (higher  $\mu_2$ ).

## 5 M/L RATIOS

We found two classes of models providing a good match to the observed stacked spectra:

- (i) Models with a constant, Salpeter (1955) IMF;
- (ii) Models with the bimodal IMF by Vazdekis et al. (1997, 2003), with a slope switching from an initial  $\mu_1$  value (top-heavy) to a different one (bottom heavy) after a time  $t_{switch} = 0.1$  Gyr.

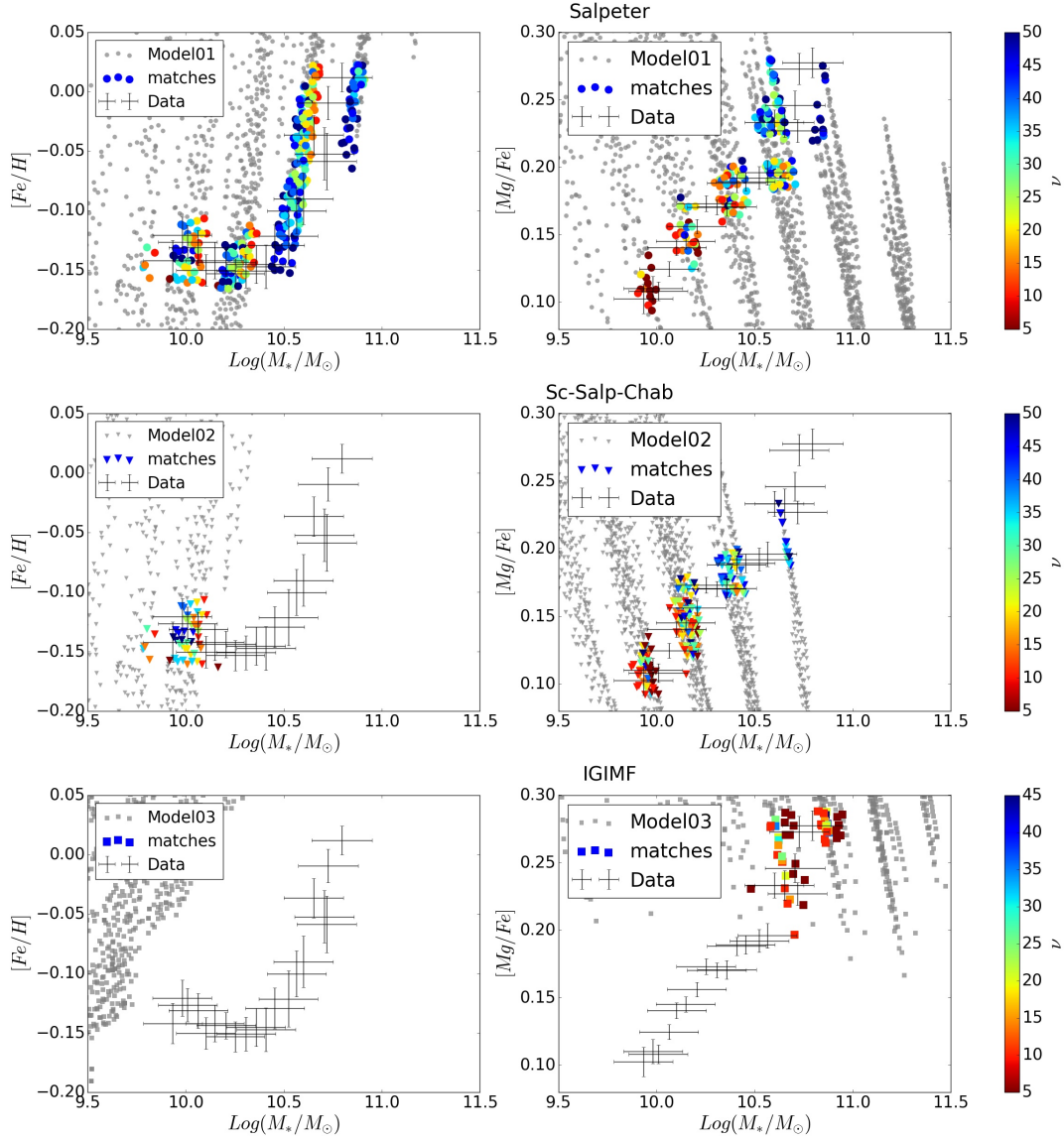


**Figure 9.** Comparison between data and Models01 (top row), 02 (central row) and 03 (bottom row) for the  $[Fe/H]$  and  $[Mg/Fe]$  abundance ratios. Matching models are color-coded according to their star formation efficiency, while not matching ones are shown with fading, smaller markers.

**Table 3.** Number of models matching the data, either for  $[Fe/H]$  or  $[Mg/Fe]$  separately, or for both of them simultaneously. In each case, the number of matches are reported in three different mass ranges referred to as "low", "middle", and "high", respectively, and for all masses ("tot").

Model	$[Fe/H]$				$[Mg/Fe]$				both			
	low	middle	high	tot	low	middle	high	tot	low	middle	high	tot
01	73	188	44	305	44	137	12	193	3	72	11	86
02	50	0	0	50	155	71	0	226	3	0	0	3
03	0	0	0	0	0	27	25	52	0	0	0	0
04	24	0	0	24	66	0	0	66	5	0	0	5
05	119	298	106	523	208	1084	505	1797	8	41	11	60

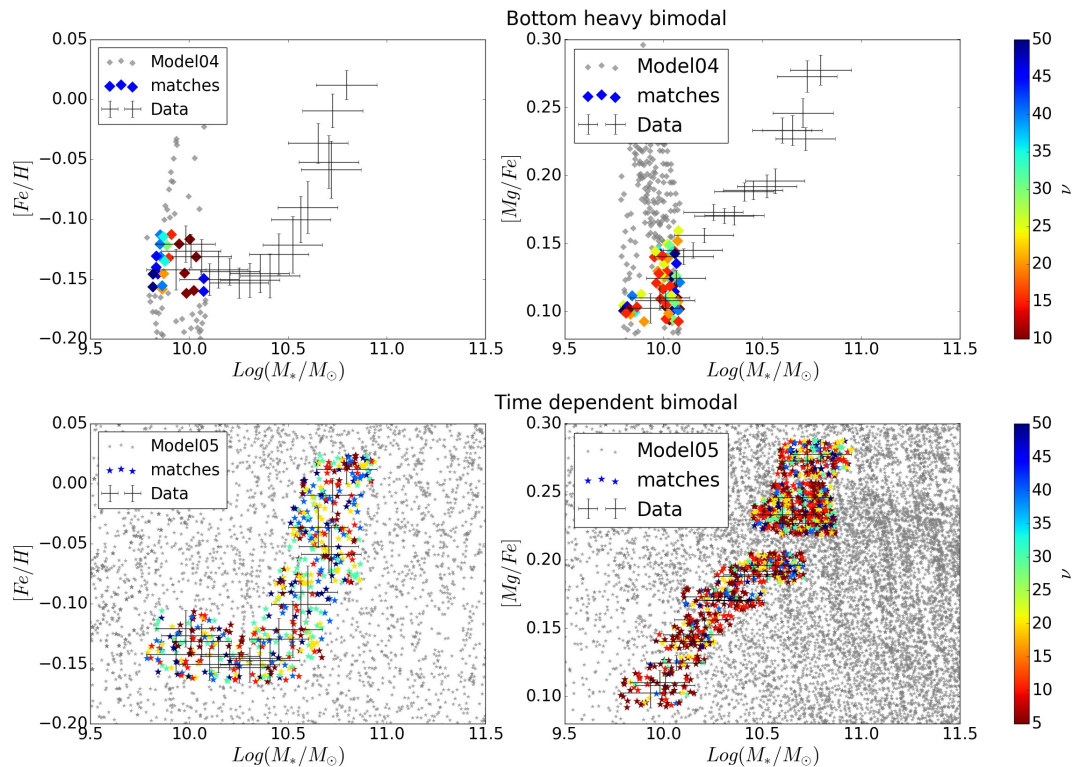


**Figure 10.** Comparison between data and Models04 (top row) and 05 (bottom row) for the  $[Fe/H]$  and  $[Mg/Fe]$  abundance ratios. Matching models are color-coded according to their star formation efficiency, while not matching ones are shown with fading, smaller markers.

As stated in the introduction of the paper, changing the IMF can have strong consequences on the properties of a galaxy, especially on its M/L ratio. In order to verify the plausibility of these two best-fitting sets of models, we investigated the expected M/L ratios by combining luminosities derived from the population synthesis code by Vincenzo et al. (2016) with the stellar masses provided by our chemical evolution code. Our predicted  $(M/L)_B$  are in the range 11.4 – 13.5 for Model01 (Salpeter IMF), and in the range 7.8 – 12.9 for Model05 (time-dependent form of the bimodal IMF) depending on the total stellar mass. These ratios are consistent with dynamical estimates (Bacon et al. 1985,  $(M/L)_B \approx 13$ ), and also with recent determinations from La Barbera et al. (2016), who showed the stellar r-band (M/L) variation with  $\sigma$  for a local sample of elliptical galaxies extracted from the ATLAS<sup>3D</sup> survey (Cappellari et al. 2013). The latter ratios were computed from the SDSS r-band luminosities, and were converted into the analogous for the B band by using EMILES SSP models (Vazdekis et al. 2015, 2016); the resulting conversion factor varies between 1.45 and 1.7, according to the mass of the galaxy and not depending on the IMF. After such conversion, their estimated  $(M/L)_B$  ratios are in the range (4.9-12.9).

The match is very good for massive galaxies, whereas our M/L are larger than the observed ones in less massive objects; in other words, since the trend of M/L with M is related to the tilt of the fundamental plane (FP), our models would imply a shallower tilt than observations. In order to reproduce the tilt, one should assume a variable IMF with stellar mass, similarly to what we did for our Model02. In

this paper we do not intend to explore the topic of the tilt of the FP, but only to verify that the average M/L ratios for our best models are close to the observed range.

## 6 ENVIRONMENT DEPENDENCE

R18 analyzed the environmental dependence of the IMF - mass relation for the SPIDER sample, investigating the impact of hierarchy (central/satellite) and of the mass of the dark matter host halo where galaxies reside.

They concluded that while age,  $[Z/H]$  and  $[Mg/Fe]$  do show a dependence on environment, the IMF slope is not influenced either by hierarchy or by host halo mass, showing a constant trend of increasing (bottom-heavier IMF) in more massive galaxies.

We re-applied all of our tests by repeating the matching procedure between models and observed galaxies, which were separated into centrals and satellites. This test gave no particular indication of a dependence of the results on hierarchy, as shown in table 4, where we reported - similarly to table 3 - the number of matching models for galaxies with different hierarchy. In the Appendix, we show plots analogous to figures 9 and 10 of section 4, showing models matching the galaxies in the observed central/satellite subsets.

## 7 SUMMARY AND CONCLUSIONS

The IMF is a crucial parameter in establishing the properties of a galaxy. In particular, from the point of view of the

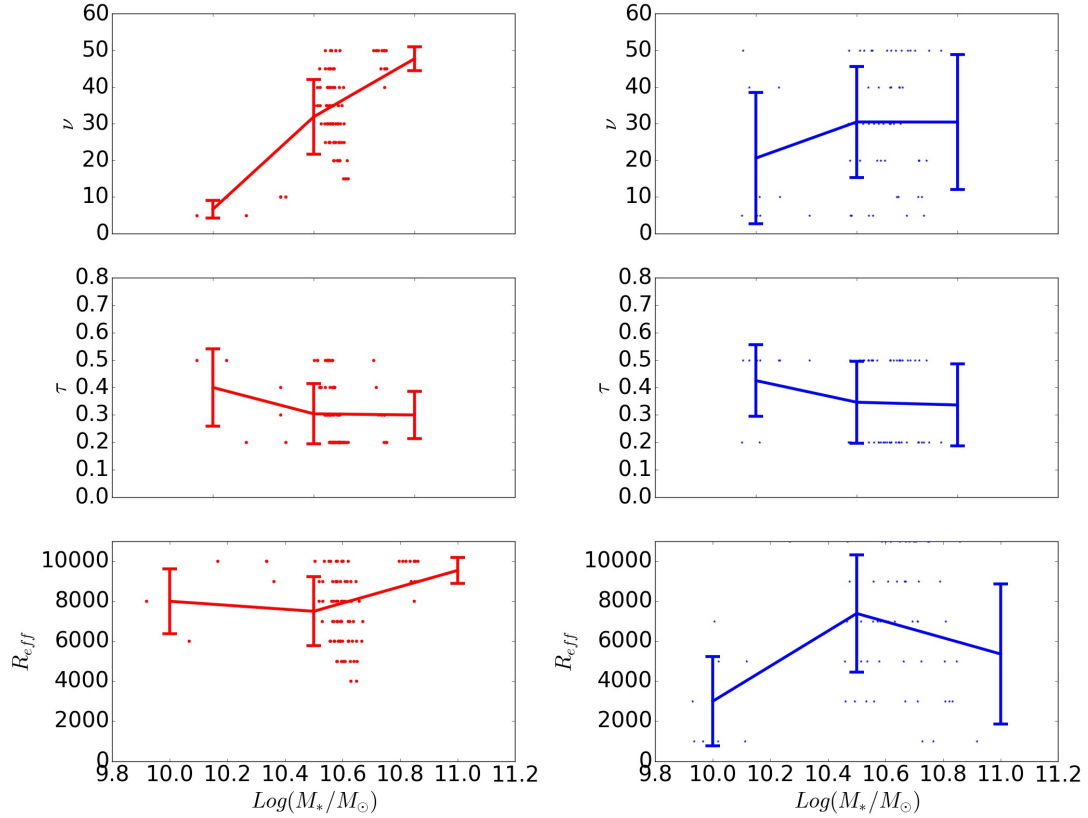


**Figure 11.** Variation with mass of the star formation efficiency (top row), infall time scale (middle row) and effective radius (bottom row) for the models matching the two abundance ratios observed in data simultaneously for a Salpeter (Model01, left) or a time-dependent bimodal (Model05, right) IMFs. The vertical error bars indicate the standard deviation of the models for the different parameters in each of the considered mass bins.

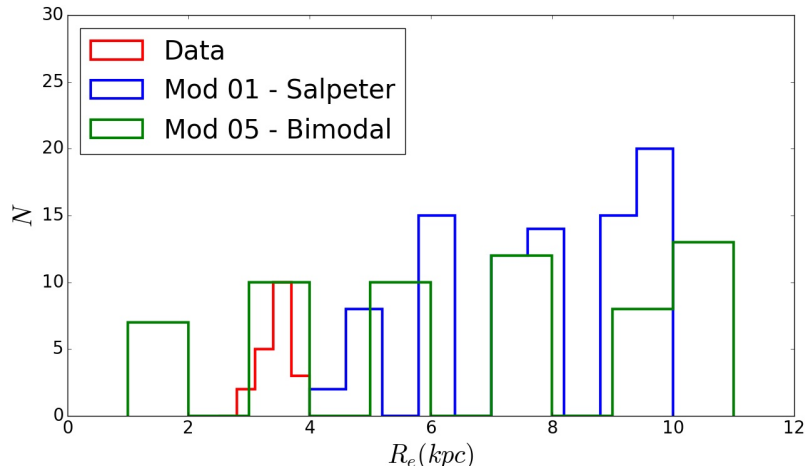


**Figure 12.** Distribution of the effective radius  $R_{eff}$  in the dataset and in the models matching the observed  $[Fe/H]$ -mass and the  $[Mg/Fe]$ -mass relations simultaneously

chemical properties, the variation of the ratio between low mass and massive stars induced by different IMFs has a very significant effect on the  $[\alpha/Fe]$  abundance ratios.

In this work, we extended our previous investigation of the effects of IMF on the chemical evolution of elliptical galaxies, by testing the same implementations of the initial mass function used in De Masi et al. (2018), plus two forms of the

bimodal IMF by Vazdekis et al. (1997, 2003). Specifically, a form becoming bottom-heavier in more massive galaxies, as suggested in Ferreras et al. (2013); La Barbera et al. (2013), and an explicitly time-dependent form of the latter, switching from top-heavy to bottom-heavy after a time  $t_{switch}$  Ferreras et al. (2015); Weidner et al. (2013). We implemented these new IMFs into our chemical evolution code

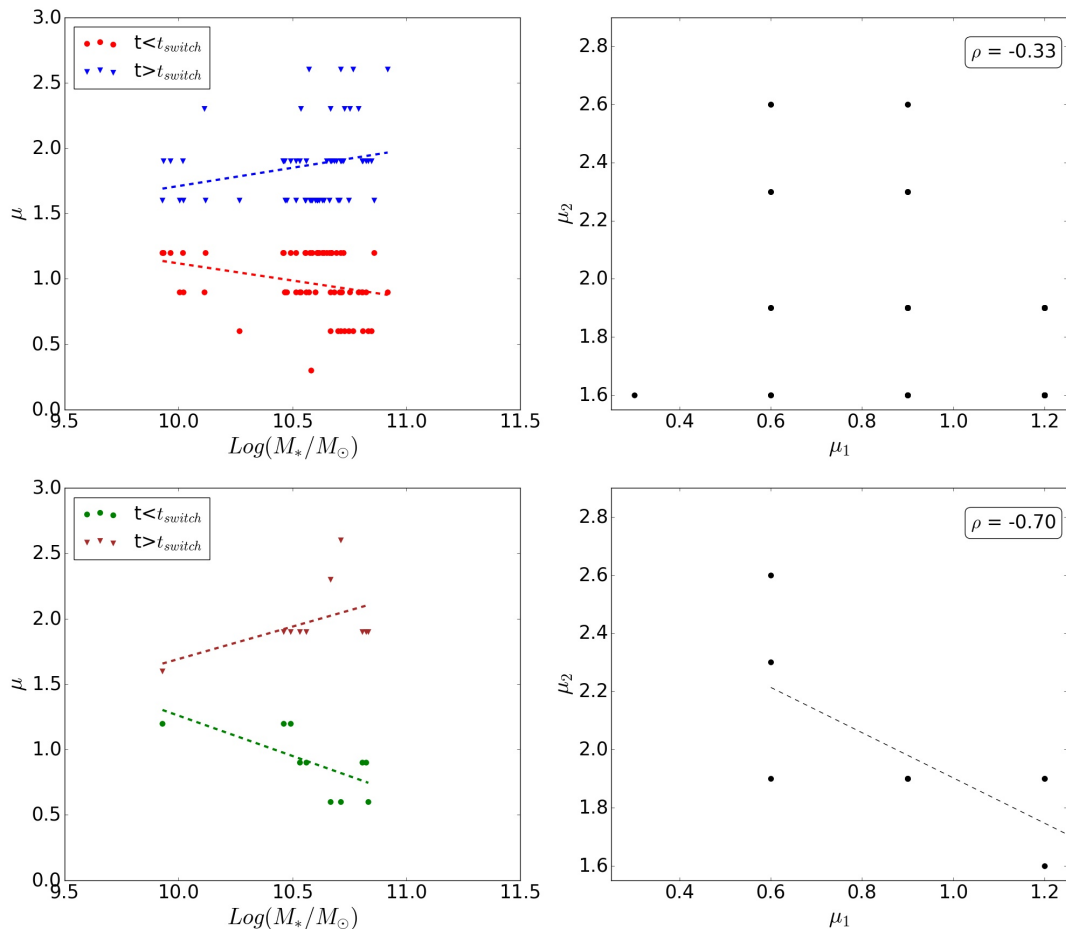


**Figure 13.** Properties of the time-dependent bimodal models matching the observed  $[Fe/H]$ -mass and the  $[Mg/Fe]$ -mass relations simultaneously. In the left column, we show the variation with mass of the IMF slope before and after the switch for models with all effective radii  $R_{eff}$  (top) and with  $R_{eff}$  matching observations (bottom). In the right column, the correlation between the slope before ( $\mu_1$ ) and after the switch ( $\mu_2$ ) is shown, again for all models (top) and only for the ones with  $R_{eff}$  compatible with observations (bottom).

**Table 4.** Number of models matching the data, either for  $[Fe/H]$  or  $[Mg/Fe]$  separately, or for both of them simultaneously. We show the number matches between models and galaxies, for the whole dataset (columns 1-3), for central galaxies only (4-6) and satellites (7-9), respectively.

Model	All			Central			Satellites		
	$[Fe/H]$	$[Mg/Fe]$	both	$[Fe/H]$	$[Mg/Fe]$	both	$[Fe/H]$	$[Mg/Fe]$	both
01	305	193	86	309	193	76	342	204	93
02	50	226	3	62	194	1	67	284	9
03	0	52	0	0	61	0	0	14	0
04	24	66	5	30	43	8	23	82	7
05	523	1797	60	510	1730	57	498	1304	46

for ellipticals, and tested its predictions against a dataset of early-type galaxies extracted from the SPIDER sample (La Barbera et al. 2010). For each IMF form, we generated models by varying all parameters of the code over a grid of values, and selected the best ones matching the observed  $[Fe/H]$ -mass and the  $[Mg/Fe]$ -mass relations within the errors on masses and chemical ratios.

All IMF choices provided models matching the data at least in some limited mass bins. However, only two scenarios provided models able to fit the two observed relations simultaneously. The models with a fixed, Salpeter IMF confirmed

that “downsizing” in star formation is required to match the data, meaning that more massive galaxies are characterized by a more efficient, shorter period of star formation (Matteucci 1994; Matteucci et al. 1998; Pipino & Matteucci 2004). The same result can be obtained by models with the time-dependent bimodal IMF.

In the first case, we obtained a crucial difference with the previous work, in that we no longer found evidence to advocate for a change in the IMF. This discrepancy can be accounted for a few main reasons:

- Simply, the use of a different dataset, characterized by a different slope of the mass-metallicity and  $[\alpha/Fe]$  relations;
- In [De Masi et al. \(2018\)](#), the main indication for the need of a IMF variation came from the analysis of the spectral indices  $Mg_2$  and  $\langle Fe \rangle$ , which we derived from the average abundances of the stellar population by applying the calibration relations by [Tantalo et al. \(1998\)](#). Since different calibrations generally yield different results ([Pipino & Matteucci 2004](#)), this procedure is always plagued by uncertainties, so that results based on such a comparison should be taken with a grain of salt.
- One of the main problems one has to deal with when comparing models with data lies in the operational definition of the various considered quantities. Our model directly provides us with the abundances of single chemical elements, whereas the abundance ratios reported for the objects in the catalog are often resulting from other quantities (see section 2 for the definitions of  $[Fe/H]$  and  $[Mg/Fe]$  adopted in this case). We always tried to be consistent in the comparison, and derived similar quantities from our models by adopting the same definitions as in the observed data. However, this means that the comparison of a given abundance ratio performed on two different catalogs may lead to a discrepancy in the resulting trends.

In spite of this difference, we confirmed the main result that, as far as the chemical properties of ellipticals are concerned, scenarios involving IMFs which are bottom-heavier through the whole evolution of more massive galaxies should be discarded, since they invariably lead to drastic underestimation of the values of  $[\alpha/Fe]$  ratios.

Regarding this point, the second successful scenario we described, i.e. a time-dependent bimodal IMF, allows us to reconcile the indications obtained from chemical abundances (i.e., higher  $[\alpha/Fe]$  ratios in massive galaxies) with the results derived from the spectra of stellar population of ellipticals, favoring bottom-heavier IMFs. It should be noted that this IMF is top-heavy in the first period of the chemical evolution of galaxies, thus accounting for the characteristic  $[\alpha/Fe]$  trends with mass, and then switch to a different, bottom-heavy form after a given time (0.1 *Gyr*). This bottom-heavy phase would account for observations, as IMF-sensitive features in the integrated spectra of ETGs at  $z \approx 0$  are dominated by stars still alive at the present time, i.e. less massive stars, whereas the more massive ones, born during the initial top-heavier phase, do not contribute to the spectra since they died a long time ago. We tested different possible values for the switching time, but said switching was always found to take place at the same time, specifically at the earliest possible one ( $\approx 0.1$  Gyr). This, again, is in accordance with observations, since ellipticals are old objects, and consequently the IMF constraints we observe at the present time are related to old stellar populations.

Whereas the bimodal IMFs in lower mass galaxies mostly present slopes similar to a canonical Kroupa IMF ( $\gamma \approx 1.3$ ), more massive ones span a wider range of values, ranging from  $\mu_1 = 0.5$  (top-heavier) before the switch to  $\mu_2 = 2.6$  (bottom-heavier) after. When considering a further selection of the models, based on their effective radii, these trends are preserved, and a weak anti-correlation between  $\mu_1$  and  $\mu_2$  is observable, suggesting that top-heavier IMFs (lower  $\mu_1$  value) before the switch correspond to bottom-heavier ones

(higher  $\mu_2$ ) after the switch. This supports the idea that when the IMF is top-heavy in a highly turbulent medium (such as the central regions of massive ETGs), the injection of energy into the ISM is so strong to possibly induce fragmentation to low-mass scales, i.e. a bottom-heavy distribution (see, for example, [Ferreras et al. 2015](#)).

Finally, we decided to investigate the M/L ratios of these two sets of models, to obtain another, independent constraint on their reliability, by combining our masses with luminosities from the population synthesis model by [Vincenzo et al. \(2016\)](#). Our M/L ratios are consistent with the average ones presented in [Cappellari et al. \(2013\)](#); [La Barbera et al. \(2016\)](#) (after converting the latter to the same photometric band we used). We are unable to reproduce the observed trend of higher M/L ratios with mass, which could be achieved by assuming a further mass dependence of the IMF. Here, however, we do not intend to reproduce the variation of the M/L ratios, but only to verify that our adopted IMFs reproduce the average observed ratios.

Finally, we repeated all the tests with a different version of the dataset, where the mass stacking was performed by separating central and satellites galaxies; the obtained results, however, did not show any significant difference, thus reinforcing the idea that the IMF is an intrinsic galaxy property, and is not affected by other “external” effects (such as the environment, where galaxies reside).

## ACKNOWLEDGEMENTS

CDM and FM acknowledge research funds from the University of Trieste (FRA2016). FLB acknowledges support from grant AYA2016-77237-C3-1-P from the Spanish Ministry of Economy and Competitiveness (MINECO).

## REFERENCES

- Arrigoni M., Trager S. C., Somerville R. S., Gibson B. K., 2010, *MNRAS*, **402**, 173
- Auger M. W., Treu T., Gavazzi R., Bolton A. S., Koopmans L. V. E., Marshall P. J., 2010, *ApJ*, **721**, L163
- Bacon R., Monnet G., Simien F., 1985, *A&A*, **152**, 315
- Barnabè M., Czoske O., Koopmans L. V., Treu T., Bolton A. S., 2011, *Monthly Notices of the Royal Astronomical Society*, **415**, 2215
- Bastian N., Covey K. R., Meyer M. R., 2010, *ARA&A*, **48**, 339
- Bell E. F., McIntosh D. H., Katz N., Weinberg M. D., 2003, *ApJS*, **149**, 289
- Bernardi M., Nichol R. C., Sheth R. K., Miller C. J., Brinkmann J., 2006, *AJ*, **131**, 1288
- Bonnell I. A., Larson R. B., Zinnecker H., 2007, *Protostars and Planets V*, pp 149–164
- Calura F., Menci N., 2009, *MNRAS*, **400**, 1347
- Cappellari M., et al., 2012, *Nature*, **484**, 485
- Cappellari M., et al., 2013, *MNRAS*, **432**, 1709
- Cappellaro E., Evans R., Turatto M., 1999, *A&A*, **351**, 459
- Cenarro A., Gorgas J., Vazdekis A., Cardiel N., Peletier R., 2003, *Monthly Notices of the Royal Astronomical Society*, **339**, L12
- Chabrier G., 2003, *PASP*, **115**, 763
- Chabrier G., Hennebelle P., Charlot S., 2014, *The Astrophysical Journal*, **796**, 75
- Chiappini C., Matteucci F., Padoan P., 1997, in *Valls-Gabaud*

- D., Hendry M. A., Molaro P., Chamcham K., eds, *Astronomical Society of the Pacific Conference Series* Vol. 126, From Quantum Fluctuations to Cosmological Structures. p. 545
- Cioffi D. F., McKee C. F., Bertschinger E., 1988, *ApJ*, **334**, 252
- Conroy C., van Dokkum P., 2012a, *ApJ*, **747**, 69
- Conroy C., van Dokkum P. G., 2012b, *ApJ*, **760**, 71
- Conroy C., Graves G. J., van Dokkum P. G., 2014, *ApJ*, **780**, 33
- De Masi C., Matteucci F., Vincenzo F., 2018, *MNRAS*, **474**, 5259
- Diaz A. I., Terlevich E., Terlevich R., 1989, *MNRAS*, **239**, 325
- Dutton A. A., et al., 2011, *MNRAS*, **416**, 322
- Dutton A. A., Mendel J. T., Simard L., 2012, *MNRAS*, **422**, L33
- Dutton A. A., Macciò A. V., Mendel J. T., Simard L., 2013, *MNRAS*, **432**, 2496
- Faber S. M., French H. B., 1980, *ApJ*, **235**, 405
- Ferreras I., La Barbera F., de la Rosa I. G., Vazdekis A., de Carvalho R. R., Falcón-Barroso J., Ricciardelli E., 2013, *MNRAS*, **429**, L15
- Ferreras I., Weidner C., Vazdekis A., La Barbera F., 2015, *MNRAS*, **448**, L82
- Gargiulo I. D., et al., 2015, *MNRAS*, **446**, 3820
- Graves G. J., Schiavon R. P., 2008, *ApJS*, **177**, 446
- Greggio L., Renzini A., 1983, *A&A*, **118**, 217
- Grillo C., Gobat R., 2010, *MNRAS*, **402**, L67
- Gunawardhana M. L. P., et al., 2011, *MNRAS*, **415**, 1647
- Hopkins P. F., 2013, *Monthly Notices of the Royal Astronomical Society*, **433**, 170
- Johansson J., Thomas D., Maraston C., 2012, *MNRAS*, **421**, 1908
- Kennicutt Jr. R. C., 1998, *ApJ*, **498**, 541
- Kroupa P., 2001, *MNRAS*, **322**, 231
- Kroupa P., 2002, *Science*, **295**, 82
- Kroupa P., Weidner C., Pflamm-Altenburg J., Thies I., Dabringhausen J., Marks M., Maschberger T., 2013, *The Stellar and Sub-Stellar Initial Mass Function of Simple and Composite Populations*. p. 115, doi:10.1007/978-94-007-5612-0-4
- Krumholz M. R., 2011, *ApJ*, **743**, 110
- Kuntschner H., 2000, *MNRAS*, **315**, 184
- La Barbera F., de Carvalho R. R., de La Rosa I. G., Lopes P. A. A., Kohl-Moreira J. L., Capelato H. V., 2010, *MNRAS*, **408**, 1313
- La Barbera F., Ferreras I., Vazdekis A., de la Rosa I. G., de Carvalho R. R., Trevisan M., Falcón-Barroso J., Ricciardelli E., 2013, *MNRAS*, **433**, 3017
- La Barbera F., Vazdekis A., Ferreras I., Pasquali A., Cappellari M., Martín-Navarro I., Schönebeck F., Falcón-Barroso J., 2016, *MNRAS*, **457**, 1468
- Larson R. B., 1974, *MNRAS*, **166**, 585
- Larson R. B., 1998, *MNRAS*, **301**, 569
- Larson R. B., 2005, *MNRAS*, **359**, 211
- Matteucci F., 1994, *A&A*, **288**, 57
- Matteucci F., 2012, *Chemical Evolution of Galaxies*, doi:10.1007/978-3-642-22491-1.
- Matteucci F., Gibson B. K., 1995, *A&A*, **304**, 11
- Matteucci F., Greggio L., 1986, *A&A*, **154**, 279
- Matteucci F., Recchi S., 2001, *ApJ*, **558**, 351
- Matteucci F., Ponzoni R., Gibson B. K., 1998, *A&A*, **335**, 855
- Newman A. B., Smith R. J., Conroy C., Villaume A., van Dokkum P., 2017, *ApJ*, **845**, 157
- Okamoto T., Nagashima M., Lacey C. G., Frenk C. S., 2017, *MNRAS*, **464**, 4866
- Pagel B. E. J., Patchett B. E., 1975, *MNRAS*, **172**, 13
- Pipino A., Matteucci F., 2004, *MNRAS*, **347**, 968
- Pipino A., Matteucci F., 2008, *A&A*, **486**, 763
- Pipino A., Matteucci F., Borgani S., Biviano A., 2002, *New Astronomy*, **7**, 227
- Recchi S., Matteucci F., D'Ercole A., 2001, *MNRAS*, **322**, 800
- Recchi S., Calura F., Kroupa P., 2009, *A&A*, **499**, 711
- Renzini A., Greggio L., 2012, *Stellar populations: a guide from low to high redshift*. John Wiley & Sons
- Rosani G., Pasquali A., La Barbera F., Ferreras I., Vazdekis A., 2018, *Monthly Notices of the Royal Astronomical Society*, p. sty528
- Salpeter E. E., 1955, *ApJ*, **121**, 161
- Scalo J. M., 1986, *Fundamentals Cosmic Phys.*, **11**, 1
- Silk J., 1995, *ApJ*, **438**, L41
- Smith R. J., Lucey J. R., 2013, *MNRAS*, **434**, 1964
- Smith R. J., Lucey J. R., Conroy C., 2015, *MNRAS*, **449**, 3441
- Spiniello C., Trager S. C., Koopmans L. V. E., Chen Y. P., 2012, *ApJ*, **753**, L32
- Spiniello C., Trager S., Koopmans L. V. E., Conroy C., 2014, *MNRAS*, **438**, 1483
- Tantalo R., Chiosi C., Bressan A., 1998, *A&A*, **333**, 419
- Thomas D., Greggio L., Bender R., 1999, *MNRAS*, **302**, 537
- Thomas D., Maraston C., Bender R., Mendes de Oliveira C., 2005, *ApJ*, **621**, 673
- Thomas D., Maraston C., Schawinski K., Sarzi M., Silk J., 2010, *MNRAS*, **404**, 1775
- Trager S. C., Worthey G., Faber S. M., Burstein D., González J. J., 1998, *ApJS*, **116**, 1
- Trager S. C., Faber S. M., Worthey G., González J. J., 2000, *AJ*, **120**, 165
- Treu T., Auger M. W., Koopmans L. V. E., Gavazzi R., Marshall P. J., Bolton A. S., 2010, *ApJ*, **709**, 1195
- Vazdekis A., Peletier R. F., Beckman J. E., Casuso E., 1997, *ApJS*, **111**, 203
- Vazdekis A., Cenarro A. J., Gorgas J., Cardiel N., Peletier R. F., 2003, *MNRAS*, **340**, 1317
- Vazdekis A., et al., 2015, *MNRAS*, **449**, 1177
- Vazdekis A., Koleva M., Ricciardelli E., Röck B., Falcón-Barroso J., 2016, *MNRAS*, **463**, 3409
- Vincenzo F., Matteucci F., Vattakunnel S., Lanfranchi G. A., 2014, *MNRAS*, **441**, 2815
- Vincenzo F., Matteucci F., Recchi S., Calura F., McWilliam A., Lanfranchi G. A., 2015, *MNRAS*, **449**, 1327
- Vincenzo F., Matteucci F., de Boer T. J. L., Cignoni M., Tosi M., 2016, *MNRAS*, **460**, 2238
- Wang L., et al., 2014, *MNRAS*, **439**, 611
- Weidner C., Kroupa P., Bonnell I. A. D., 2010, *MNRAS*, **401**, 275
- Weidner C., Kroupa P., Pflamm-Altenburg J., 2011, *MNRAS*, **412**, 979
- Weidner C., Ferreras I., Vazdekis A., La Barbera F., 2013, *MNRAS*, **435**, 2274
- Whelan J., Iben Jr. I., 1973, *ApJ*, **186**, 1007
- Wing R. F., Ford Jr. W. K., 1969, *PASP*, **81**, 527
- Yang X., Mo H. J., van den Bosch F. C., Pasquali A., Li C., Barden M., 2007, *ApJ*, **671**, 153
- van Dokkum P. G., Conroy C., 2010, *Nature*, **468**, 940
- van Dokkum P. G., Conroy C., 2011, *ApJ*, **735**, L13

## APPENDIX A: MATCHES FOR CENTRAL/SATELLITES

As reported in section 6, we analyzed the impact of hierarchy on the matching between models and data. Figures A1 to A4 are analogous to figures 9 and 10, and show the results of the matching procedure with the subset of central/satellite galaxies in the dataset. As mentioned in the text, no significant difference with the general case (where we did not divide galaxies according to their hierarchy) is noticeable.

This paper has been typeset from a  $\text{\TeX}/\text{\LaTeX}$  file prepared by the author.

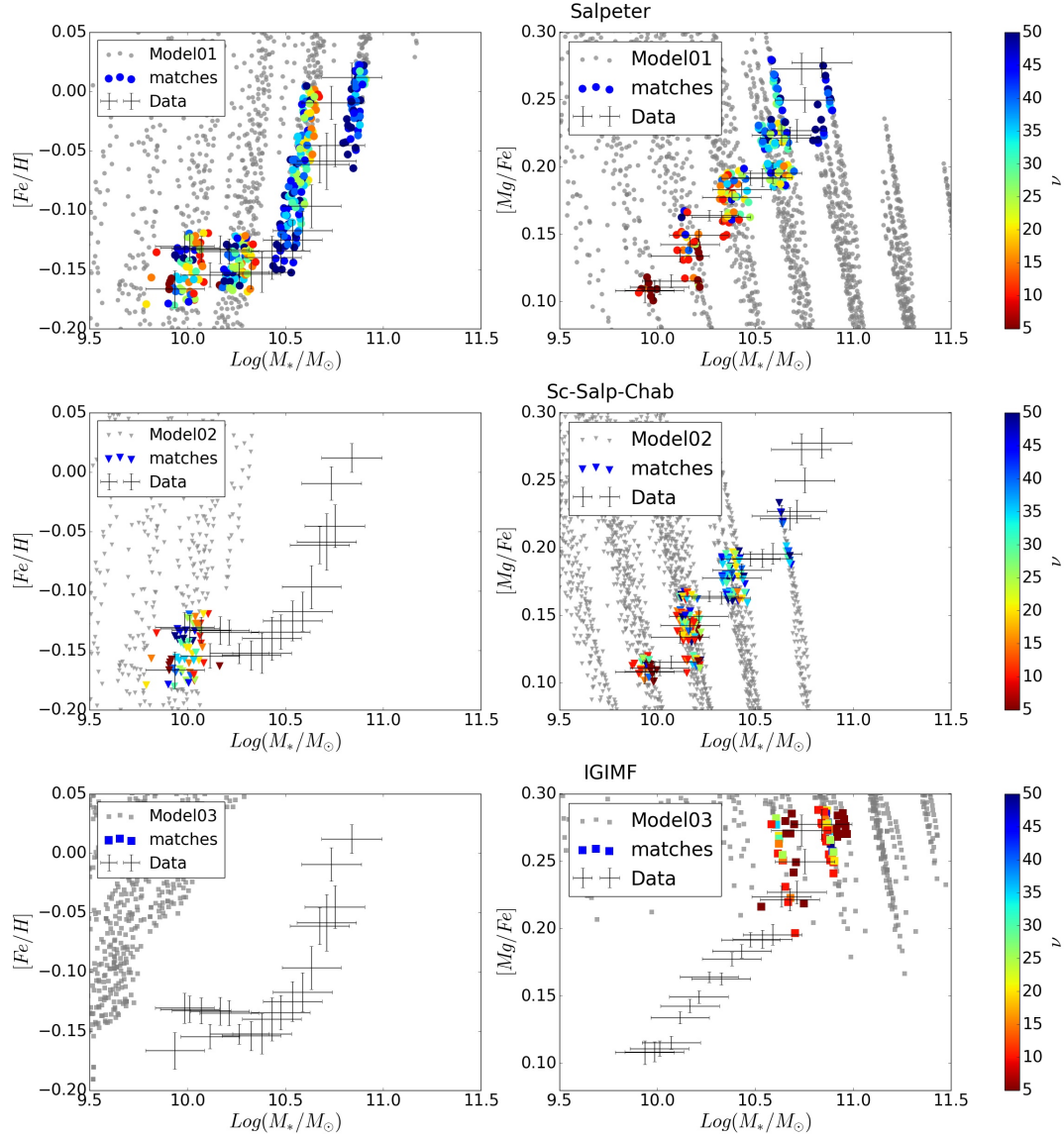


**Figure A1.** Comparison between central galaxies in the dataset data and Models01 (top row), 02 (central row) and 03 (bottom row) for the  $[Fe/H]$  and  $[Mg/Fe]$  abundance ratios. Matching models are color-coded according to their star formation efficiency, while not matching ones are shown with fading, smaller markers.

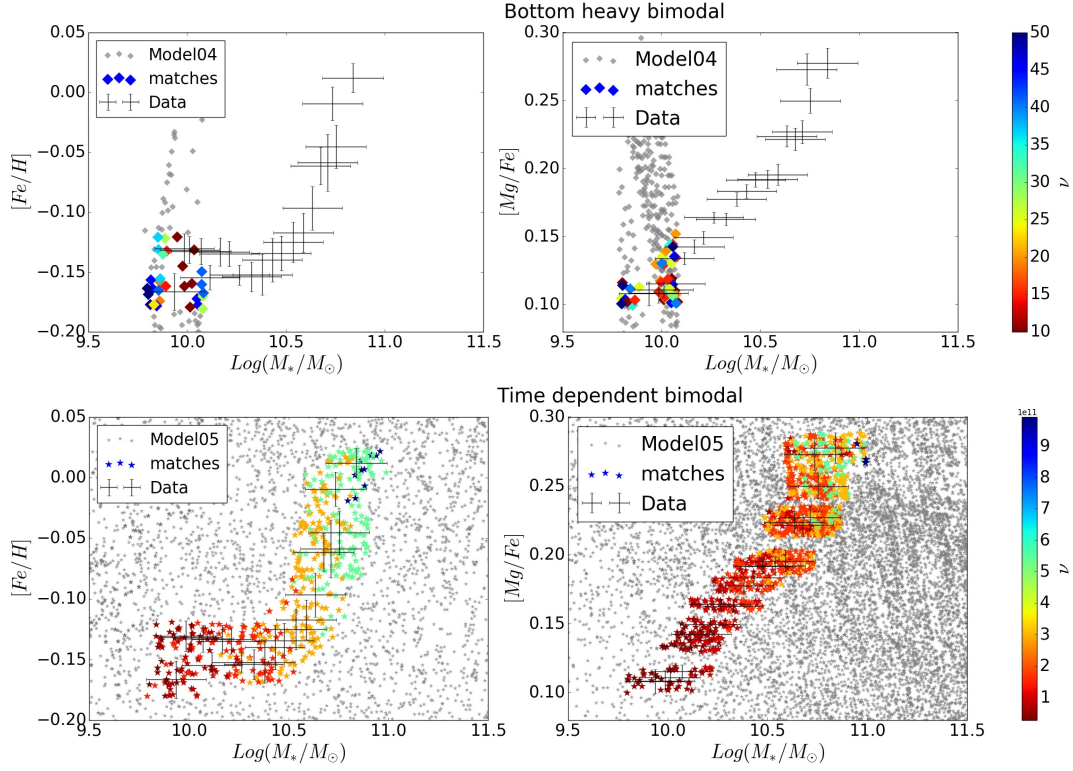


**Figure A2.** Comparison between central galaxies in the dataset and Models04 (top row) and 05 (bottom row) for the  $[Fe/H]$  and  $[Mg/Fe]$  abundance ratios. Matching models are color-coded according to their star formation efficiency, while not matching ones are shown with fading, smaller markers.

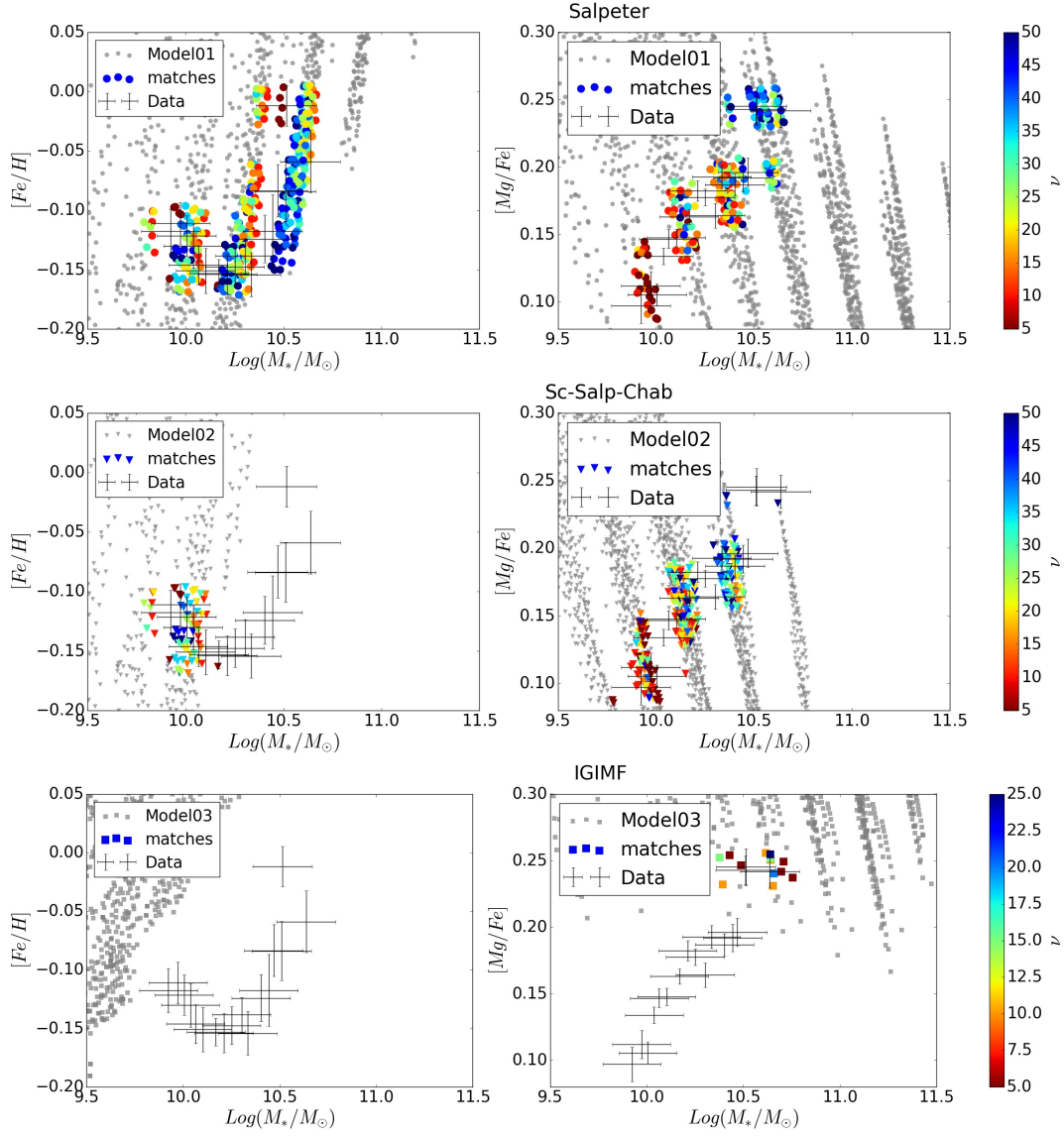


**Figure A3.** Comparison between satellite galaxies in the dataset data and Models01 (top row), 02 (central row) and 03 (bottom row) for the  $[Fe/H]$  and  $[Mg/Fe]$  abundance ratios. Matching models are color-coded according to their star formation efficiency, while not matching ones are shown with fading, smaller markers.

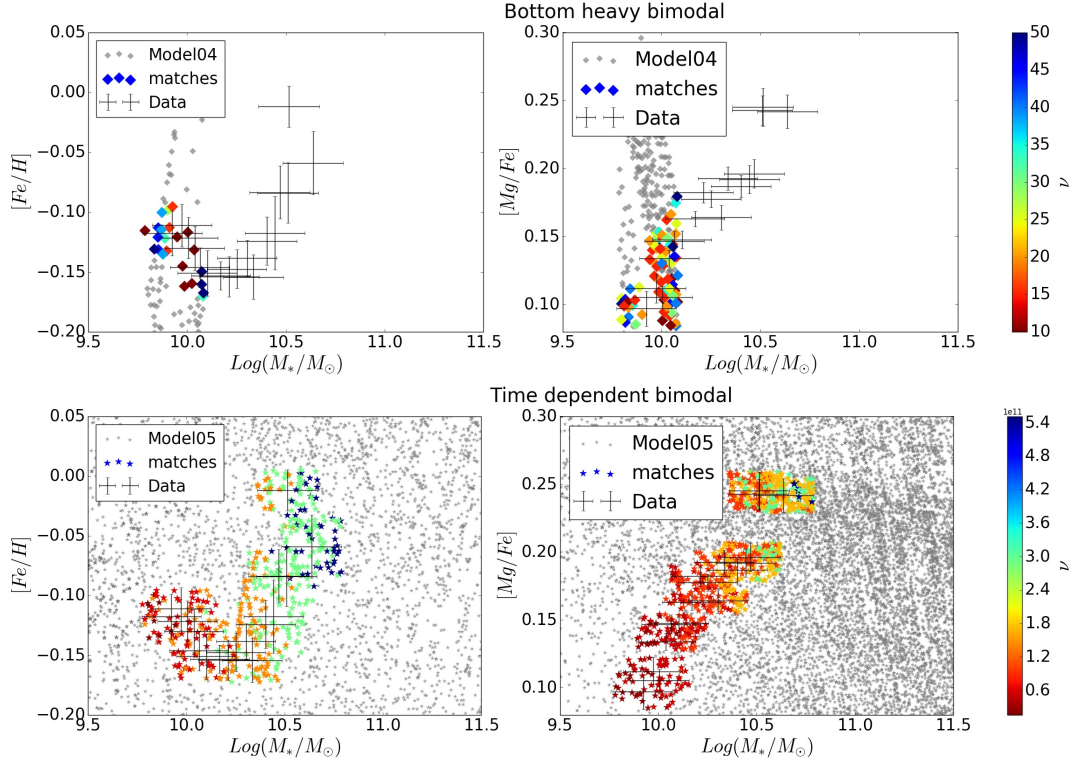


**Figure A4.** Comparison between satellite galaxies in the dataset and Models04 (top row) and 05 (bottom row) for the  $[Fe/H]$  and  $[Mg/Fe]$  abundance ratios. Matching models are color-coded according to their star formation efficiency, while not matching ones are shown with fading, smaller markers.